Pramana – J. Phys. (2019) 93:32
https://doi.org/10.1007/s12043-019-1794-3

The synthesis and study of structural, optical and electrical behaviours of tin oxide/polyaniline (SnO_2/PANI) nanocomposites

B SINGH* and B DAS

Advanced Materials Research Lab, Department of Physics, University of Lucknow, Lucknow 226 007, India
*Corresponding author. E-mail: bs2801514@gmail.com

MS received 17 September 2018; revised 25 December 2018; accepted 8 February 2019;
published online 30 May 2019

Abstract. A series of tin oxide (SnO_2)/polyaniline (PANI) nanocomposites with loading of different wt% of PANI were synthesised using a solution-based processing method for improving the structural and physical properties of tin oxide. The effect of PANI loading on the gross structure, surface morphology, optical properties and electrical properties of SnO_2/PANI nanocomposites was investigated. The scanning electron micrographs (SEM) show congruent dispersal of PANI in the tin oxide matrix where the gross/average structure is unchanged as revealed by powder X-ray diffraction (PXRD). A slight change in the lattice parameter of the pristine rutile crystalline structure SnO_2 and its nanocomposites has been recorded. However, the crystallite size has been found to decrease from 60 to 40 nm with different wt% loading of PANI. The presence of characteristic Fourier transform infrared (FT-IR) peaks dovetail to C–H, C=C, NH_2, C–C and the energy-dispersive analysis of X-rays (EDAX) confirm the development of the PANI nanocomposite. Photoluminescence (PL) spectroscopic study shows the gradual decrement in the intensity of the emission peak at 611 nm due to the disappearance of surface defects associated with oxygen vacancies. The uniform dispersion of PANI at the nanoscale significantly enhanced the electrical properties, e.g. four orders of magnitude changes in electrical conductivity and carrier mobility.

Keywords. X-ray diffraction; polymer-based composites.

PACS Nos 61.05.cp; 81.05.Qk

1. Introduction

Recently, efforts have been made to synthesise nanocomposites of different metal or metal oxide nanoparticles having different structures, such as nanofibres (NFs), nanowires (NWs), nanobelts (NBs) and nanotubes (NTs) with conducting polymers having interesting functionalities, e.g. polyaniline (PANI). In the natural form, PANI is a base, but by the addition of acids such as hydrochloric acid and camphorsulphonic acid of various concentrations, its conductivity was changed as reported by Blinova and Stejskal [1]. PANI has more prominence because it can be easily synthesised, its cost is reasonable, it has improved properties and it has excellent environmental stability [2]. PANI has exclusive chemical, electrical, environmental, thermal, electrochemical, electronic, optical and electro-optical properties [3]. PANI is one of the most extensively studied polymeric semiconductors, which is of special interest for developing optical and electric devices, electrode materials, conducting coatings, etc. [4]. Nanosized particles of various shapes and structures have been found to possess amazing physical and chemical properties and have shown a number of fascinating potential applications in a wide range of fields such as electronics, magnetic and optoelectronics, biomedical, pharmaceutical, cosmetics, energy, environmental, catalytic and space technology [5,6]. SnO_2 is an n-type semiconductor having a band gap of 3.6 eV at 300 K, whereas PANI is a typical p-type conductive polymer [7]. Researchers have investigated composites of PANI with inorganic materials for catalysis, sensors and other similar applications [8]. Metal oxide non-materials are probably the most diverse, rich and multifunctional materials with properties covering almost all aspects of chemistry, materials science and solid-state physics [9,10]. Among them, 4d transition metal oxides, i.e. SnO_2 and In_2O_3 are the rarest conductors compared to semiconductors or superconductors which have an optical transparency of more than 97%, corresponding to the visible range (film thickness = 0.1–1.0 μm) and have a resistivity of 10^{-4}–10^6 Ω cm, remarkably lower than most of

the semiconductors (10^{-3}–$10^{9}\ \Omega$ cm). Nominally pure SnO_2 has a carrier concentration of up to 10^{20} cm^3 compared to that of semimetals (10^{17}–10^{20} cm^3). This high electron concentration has already been explained by oxygen vacancies (V_O) and tin interstitials (S_{ni}). Thus, tin oxide having a wide band gap of $E_g = 3.6$ eV exhibits contradictory high metallic conductivity due to its massive non-stoichiometry [11]. Later, several studies have been reported on SnO_2-based gas sensors, dye-sensitised solar cells, optical–optoelectronic and hybrid microelectronic devices [12,13]. However, for further improving the performance of devices based on bulk SnO_2, there are two ways, either by synthesising nanostructures of SnO_2 or by metal doping (substitution) or making nanocomposites of SnO_2 with conducting polymers. So far, the synthesis of nanostructures of SnO_2 such as nanocrystals, nanowires, nanobelts and nanotubes, have been reported [14]. Among them, nanocrystals are widely used, owing to their size-dependent optical and electronic properties. The properties of SnO_2 nanoparticles are different from bulk materials (almost insulator-like), especially when their size is smaller than the Bohr exaction radius due to the quantum size effect [15]. The conducting polymers are a new group of synthetic polymers that display unusual electronic properties such as low ionisation potentials, high electron affinities as well as a combination of both chemical and mechanical properties of metals and semiconductors [16]. Among them, PANI is one of the most beneficial conjugated p-electron polymers which has also been investigated for its wide potential utilisation such as gas sensors, solar cells and electrochromic devices with the aim to further improve the performance of solar cells [17–19].

2. Experimental details

2.1 *Synthesis of the SnO_2, PANI and SnO_2/PANI nanocomposites*

All chemicals, e.g. aniline ($C_6H_5NH_2$), tin chloride ($SnCl_2{\cdot}2H_2O$), ammonium peroxidisulphate (APS) ($H_8N_2O_8S_2$) or $(NH_4)_2S_2O_8$, methanol solution, HCl, acetone, NH_4OH solution and distilled water used in the present investigation were obtained from MERC, India Ltd. First, pure SnO_2 was prepared by the co-precipitation method. Initially, 50 ml of 1 M solution of $SnCl_2 \cdot 2H_2O$ was stirred using a magnetic stirrer for 2 h and then four pellets (∼1.0 g) of NaOH were mixed and again the solution was magnetically stirred for 2 h for complete precipitation. After filtering the precipitate, it was dried at 500°C for 12 h. The dried precipitate was ground using a mortar and pestle for 6 h and calcined at 700°C for 4 h. After calcination, it was again ground for 5 h and calcined at 800°C for 4 h. Finally, the pellets of SnO_2 were made by applying 3000−4000 kg/cm^2 pressure in a hydraulic pressure machine and sintered at 900°C for 10 h.

About 50 ml solution of 1 M concentration of both aniline hydrochloride ($C_6H_5NH_2Cl$) and APS were made by dissolving in double distilled H_2O in a volumetric flask individually. The solutions prepared as above were kept for 1 h at room temperature and were later mixed with a brief stirring and left to rest to polymerise. The colour of the solution changed to dark green after a few minutes. After 24 h, a green precipitate of emeraldine base PANI formed was filtered and washed three times with distilled H_2O and 100 ml of 0.1 M HCl to discard unreacted aniline. After this, the precipitate was washed thrice with acetone to remove water molecules and to eliminate the leftover organic impurities. It was then dried under vacuum (10^{-3} torr) in a furnace for 3 h at 70°C. The precipitate was finally converted into a fine powder by grinding it up to 5–6 h and then this powder was sintered in a furnace at 90°C.

The SnO_2/PANI nanocomposite was synthesised by a thorough mixing of different wt% of PANI in SnO_2 powder using a mortar and pestle. Before characterisation, the samples were pelletised by applying 3000−4000 kg/cm^2 pressure for 5 min using a hydraulic pressure machine to form pellets of 10 mm diameter and 1–3 mm thickness. Finally, all pellets were sintered in a furnace at 100°C for 2 h.

2.2 *Characterisation*

All the prepared pure SnO_2, PANI and SnO_2/PANI nanocomposites were epitomised by X-ray diffraction (XRD), scanning electron microscopy (SEM) coupled with energy-dispersive analysis of X-rays (EDAX), Fourier transform infrared (FT-IR) and photoluminescence (PL) spectroscopies and Hall measurements.

2.2.1 *Structural/microstructural characterisation.* The gross (average) structural, microstructural and surface morphological characteristics were studied by powder X-ray diffraction (PXRD) and SEM, respectively.

2.2.1.1 *PXRD studies.* PXRD of the nanocomposites were recorded on a Rigaku X-ray diffractometer (Ultima IV, Japan), using CuKα radiation ($\lambda = 0.15406$ nm) at 40 kV and 40 mA. The X-ray was produced using a sealed Cu-tube, and the wavelength of CuKα radiation was 1.54060 Å. The scattered X-rays were detected using a fast counting scintillation detector at

UGC-DAE CSR (consortium for scientific research), Indore (IUC).

2.2.1.2 *SEM.* The surface morphology and dispersion of PANI in the SnO_2 matrix as well as the elemental analysis were carried out with a JEOL scanning electron microscope coupled with an energy-dispersive X-ray spectroscopic (EDS) detector (SEM, JSM-6380LV) with an accelerating voltage of 20 kV at Inter University Accelerator Centre (IUAC), New Delhi. The sample surfaces were coated with 10 nm thick films of gold (Au) metal by DC sputtering prior to SEM observations.

2.2.2 *Optical characterisation.* FT-IR spectroscopy is an informative approach for studying the functional groups as well as the nature of chemical bonds attached to the SnO_2/PANI nanocomposites. The infrared spectrum of the nanocomposite samples pelletised with KBr was measured at Department of Physics, University of Lucknow using a FT-IR spectrometer Bruker (Tensor 27) having a resolution of 5 cm^{-1} and the scanning coverage was from 4000 to 400 cm^{-1}. The specimens were dispersed into the KBr powder by mortar and compressed into a pellet form. PL spectroscopy is a well-established technique for studying the optical properties of solids. PL spectra of the pure SnO_2 and the prepared SnO_2/PANI nanocomposites were recorded at room temperature (300 K) using PL spectrometer (Mechelle 900) at the Inter University Accelerator Centre (IUAC), New Delhi. This spectrograph is sensitive in the 200–1100 nm region, having a thermoelectrically cooled charge-coupled device (CCD) array-based detection system. The PL excitation is feasible either by $\lambda = 325$ or 441.6 nm line of a He–Cd laser by a sapphire window.

2.2.3 *Electrical/electronic characterisation.* In order to record the electrical/electronic properties of the pure SnO_2 and SnO_2/PANI nanocomposites with the help of Keithley's Hall effect switching card, voltmeter (2182A) and constant-current source (2400) system, Hall measurements were performed at room temperature (300 K) by measuring direct electrical current and voltage to determine the electrical resistivity (ρ), carrier concentration (n) and carrier mobility (μ) by the four-probe method, employing Van der Pauw geometry at the Inter University Accelerator Centre (IUAC), Delhi. The pellets of 10 mm diameter and approximately 2 mm thickness were mounted on a specially designed printed circuit board (PCB) containing four point probes (contacts) which were spring loaded. A highly conducting silver paint was used at the probes to get better contacts.

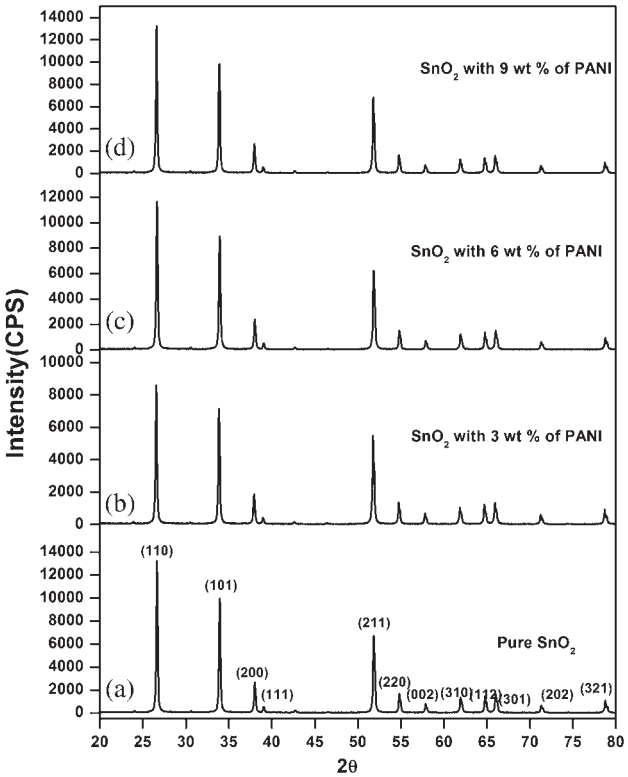

Figure 1. XRD patterns of (**a**) pure SnO_2, (**b**) 3 wt%, (**c**) 6 wt% and (**d**) 9 wt% of PANI in the SnO_2/PANI nanocomposite.

3. Results and discussion

3.1 *XRD analysis*

The representative X-ray diffraction patterns of pure SnO_2 and SnO_2/PANI nanocomposites with different PANI concentrations (3, 6 and 9 wt%) are shown in figure 1, where figure 1a represents X-ray diffraction pattern of pure SnO_2 while figures 1b–1d represent X-ray diffraction pattern of SnO_2/PANI nanocomposites at 3, 6 and 9 wt% respectively. The analysis of the powder X-ray diffractograms (PXRD) reveals that the prepared pure SnO_2 and its nanocomposites are crystalline and all tentative peaks corresponding to the tetragonal rutile-type SnO_2 phase (space group $P4_2/mnm$) are present and perfectly match with the JCPDS data (card no-077-0447). No other peaks from any kind of impurities are traced, indicating the high purity of the product. On the other hand, the synthesised pure PANI appears to be amorphous because no sharp diffraction peaks are present in the X-ray diffractogram. Furthermore, from the observed XRD pattern, the lattice constants a and c, c/a ratio, unit cell volume and crystallite size, by both Scherer formula and Williamson–Hall plot, were also calculated and their

Table 1. Lattice constants a and c, c/a ratio, unit cell volume and crystallite size of pure SnO_2 and SnO_2/PANI nanocomposites with 3, 6 and 9 wt% of PANI.

Samples	Cell constant a (Å)	Cell constant c (Å)	c/a ratio	Cell volume	Crystallite size (nm)	
					W–H plot	Scherer formula
Pristine SnO_2	4.7328	3.1838	0.6735	71.3151	57.793	58.728
SnO_2 + 3 wt% of PANI	4.7388	3.1876	0.6726	71.5814	47.70	51.677
SnO_2 + 6 wt% of PANI	4.7366	3.1862	0.6732	71.4836	44.78	48.88
SnO_2 + 9 wt% of PANI	4.7326	3.1842	0.6728	71.3181	42.32	47.465

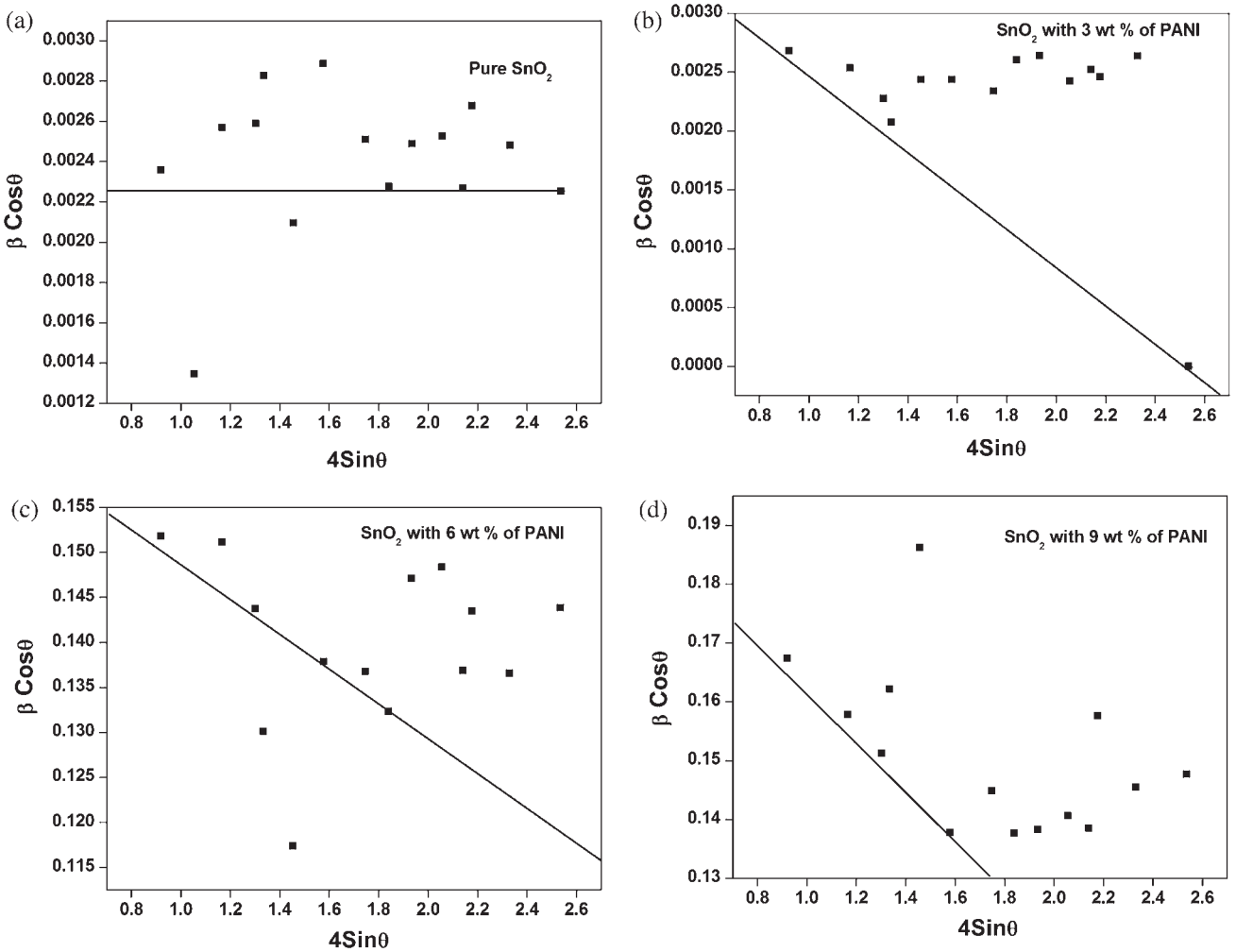

Figure 2. W–H plot of (**a**) pure SnO_2, (**b**) 3 wt%, (**c**) 6 wt% and (**d**) 9 wt% of PANI in the SnO_2/PANI nanocomposite.

values are shown in table 1. The broadening of X-ray diffraction peaks may be due to the decreasing crystallite size and the strain associated with lattice distortions and lattice defects. Williamson and Hall recommended broadening profiles due to size and strain are Lorentzian. Based on this, they derived a relation between the average crystallite size (D) and the lattice microstrain (ε) as follows:

$$\beta \cos \theta = k\lambda/D + 4\varepsilon \sin\theta, \quad (1)$$

where β is the full-width half-maxima, λ is the wavelength of the radiation (1.54060 Å for CuKα radiation), k is a constant equal to 0.94 and θ is the angle. The plot of $\beta\cos\theta$ vs. $\sin\theta$ is a straight line and the values of the crystallite size (D) and lattice strain (ε) can be obtained from the intercept and the slope of the straight line, respectively. The plots of Williamson and Hall (W–H) for pure SnO_2 and SnO_2/PANI nanocomposites with loading of different wt% (3, 6, 9 wt%) of PANI are shown in figure 2, where figure 2a represents

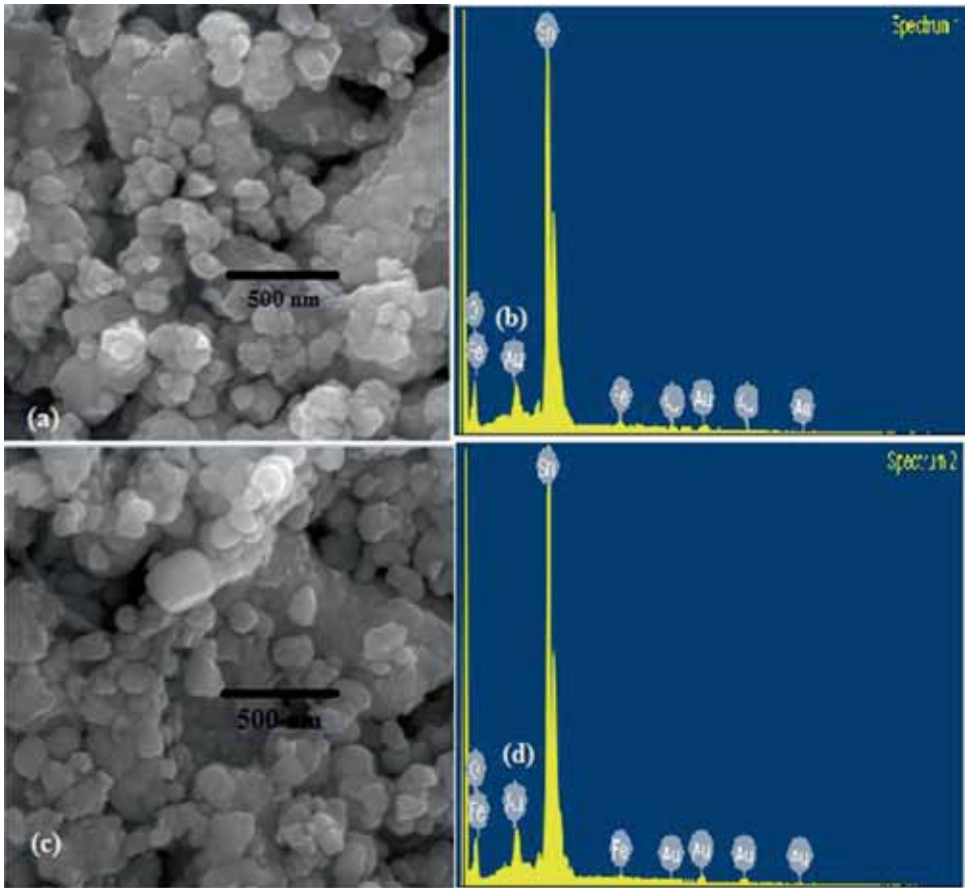

Figure 3. SEM image of (**a**) pure SnO_2, (**b**) EDAX of pure SnO_2, (**c**) SEM image of the SnO_2/PANI nanocomposite and (**d**) EDAX of the SnO_2/PANI nanocomposite.

W–H plot for pure SnO_2 while figures 2b–2d represent W–H plots of SnO_2/PANI nanocomposites at 3, 6 and 9 wt% respectively. Furthermore, the lattice constants *a* and *c* of the nanocomposites (SnO_2/PANI) for 3 wt% of PANI initially increase and then subsequently decrease as the PANI content increases from 3 to 9 wt%. The average value of the lattice parameter initially increased and later decreased, indicating that the grains present in the composite are strained, may be due to their smaller average size [20]. However, the crystallite (grain) size of the pure SnO_2 and the nanocomposites (SnO_2/PANI) were found to decrease from about 57 to 40 nm. The crystallite size of the nanocomposite decreases by the increasing wt% of PANI in SnO_2 which may be due to the applied external force, increased interaction between SnO_2 and PANI molecules and due to the adsorption of PANI molecules on the surface of SnO_2 particles [21].

3.2 *SEM/EDAX analysis*

SEM micrographs along with the EDAX spectrum of pure SnO_2 and its nanocomposite with 6 wt% of PANI are shown in figure 3, where figures 3a and 3b represent SEM image/EDAX spectrum of pure SnO_2 while figures 3c and 3d represent SEM image/EDAX spectrum of SnO_2/PANI nanocomposites at 6 wt%. The SEM micrograph shows the porous, crystalline nanostructure of pure SnO_2 and the semicrystalline structure of SnO_2/PANI nanocomposites. It can also be seen that the shape of the particles is spherical and size of the particles are in the range of 100–300 nm. The EDAX spectrum consists of all peaks corresponding to C, H, O and Sn elements present in the investigated pellets.

3.3 *FT-IR analysis*

FT-IR spectra of the pure SnO_2 and its nanocomposites with different wt% (3, 6, 9 wt%) of PANI in the transmission mode was recorded in the range $400-4000\ cm^{-1}$ as indicated in figure 4. For comparison, the approximate frequency range of various functional groups in the infrared range is also given in table 2. The tentative peak of pure SnO_2 is obtained at wave number $615\ cm^{-1}$ as shown in figure 4 which may be due to the antisymmetric Sn–O–Sn mode in SnO_2 [22] for the PANI/SnO_2 nanocomposites. Figure 4a represents

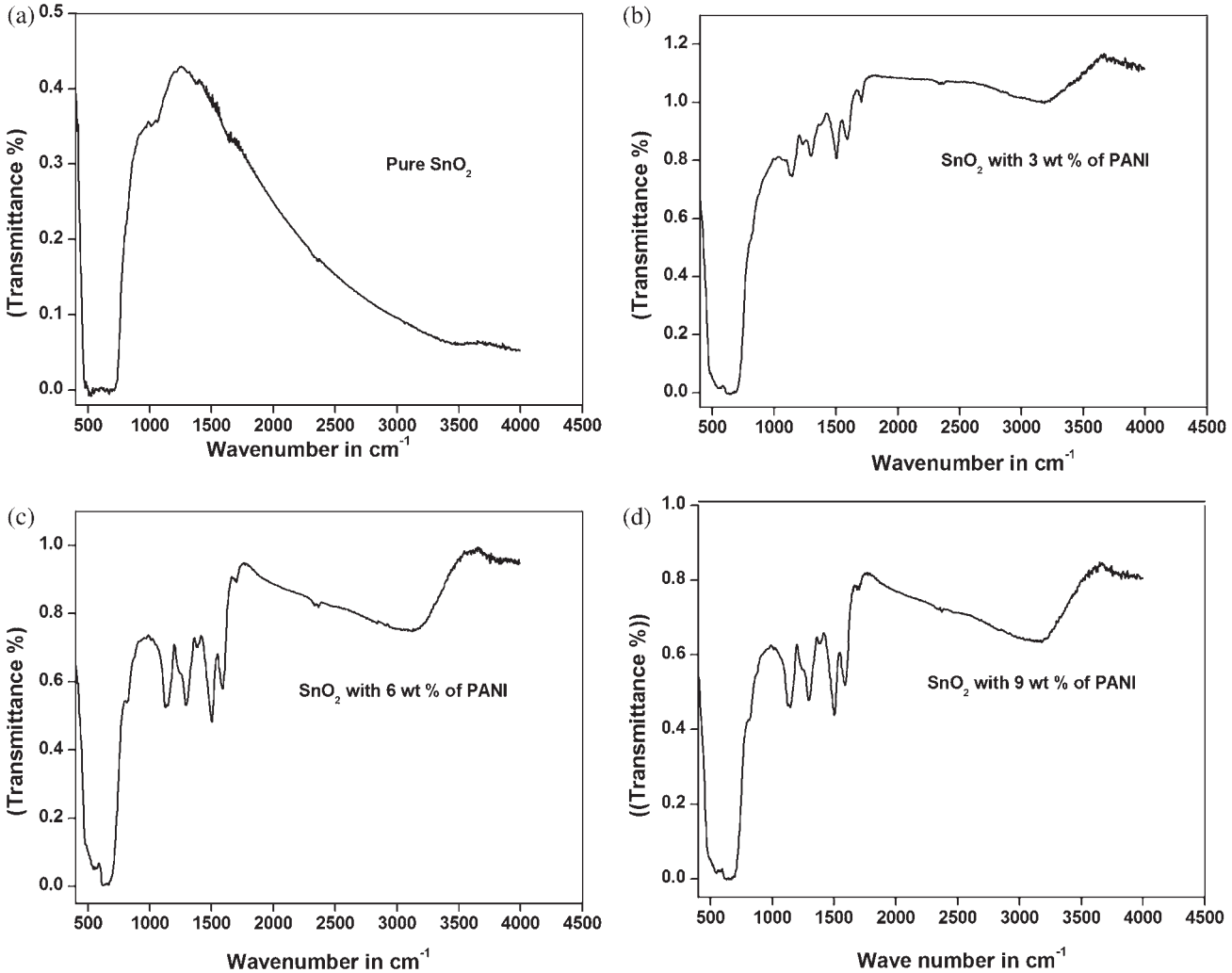

Figure 4. FT-IR spectra of (**a**) pure SnO_2, (**b**) 3 wt%, (**c**) 6 wt% and (**d**) 9 wt% of PANI in the SnO_2/PANI nanocomposite.

FT-IR spectra of pure SnO_2 while figures 4b–4d represent FT-IR spectra of SnO_2/PANI nanocomposites at 3, 6 and 9 wt% respectively. In the FT-IR spectra of the SnO_2/PANI nanocomposites, the peaks are observed at wave numbers 2300, 1780, 1660, 1555, 1450, 1300, 1206 and 995 cm^{-1} equivalent to most of the characteristic peaks for PANI. The peak at a frequency of 2300 cm^{-1} is attributed to the C–H bond stretching in PANI, whereas the peaks at 1780 cm^{-1} represent either the C–N or the C–C stretching mode for the quinoid, benzenoid rings and N–H wagging, while the peak at wave number 1660 cm^{-1} is attributed to the C=C aromatic stretching. The peak amplitude characteristic of the absorption upon stretching vibration of the quinoid ring is found to be 1450 cm^{-1} which is nearly equal to the corresponding absorption peak position of a benzene ring at 1487 cm^{-1}, which is a distinctive aspect of the conductive form of PANI. The characteristics peaks around 1481 and 1569 cm^{-1} are associated with the C=N stretching mode of quinoid rings and the C=C stretching mode of benzenoid rings, respectively, as these peaks correspond to the most characteristic peaks of PANI [23]. The peak at 1300 cm^{-1} may be associated with the C–H and C–C stretching modes and the C–H cyclic mode. The C–N stretching vibrations in the polymer chain result in the peak formation at 1206 cm^{-1}. The C–H of 1–4 tri-substituted aromatic rings is responsible for the observed peak at about 995 cm^{-1} [24–27].

3.4 *PL analysis*

PL spectra of pure SnO_2 and SnO_2/PANI nanocomposites at an excitation wavelength (λ) of 325 nm were recorded and the intensities vs. wavelength curves are shown in figure 5, where figure 5a represents PL spectra of pure SnO_2 while figures 5b–5d represent PL spectra of SnO_2/PANI nanocomposites at 3, 6 and 9 wt% respectively. All these curves show neither a blue shift nor a red shift of the emission peak, indicating no gross structural changes in the nanocomposites. However, a

Table 2. Approximate frequencies of functional groups in the infrared range.

Frequency (cm^{-1})	Types of group	Borderline group
2000–5000	X–H stretching	
	X=X=X stretching	
	Z–H stretching	
	X=X=stretching	
1400–2000	X=X stretching (aliphatic)	X–H bending
	X=X stretching (aromatic)	X–H wagging
	X=Y stretching	
1000–1400	X–X stretching	X–X stretching
	X–Y stretching	X–Y cyclic
	X=Z stretching	
	Z–H bending	
650–1000	X=X–H bending XH2 rocking	
	X–H aromatic bending	
	X–Z stretching	
400–650	X–Z bending	
	X–X and X–Y bending (in cyclic or aromatic compounds)	
	X–Br stretching	
	X–I stretching	

X and Y may be carbon, nitrogen, oxygen or fluorine, Z may be silicon, phosphorous, sulphur or chlorine.

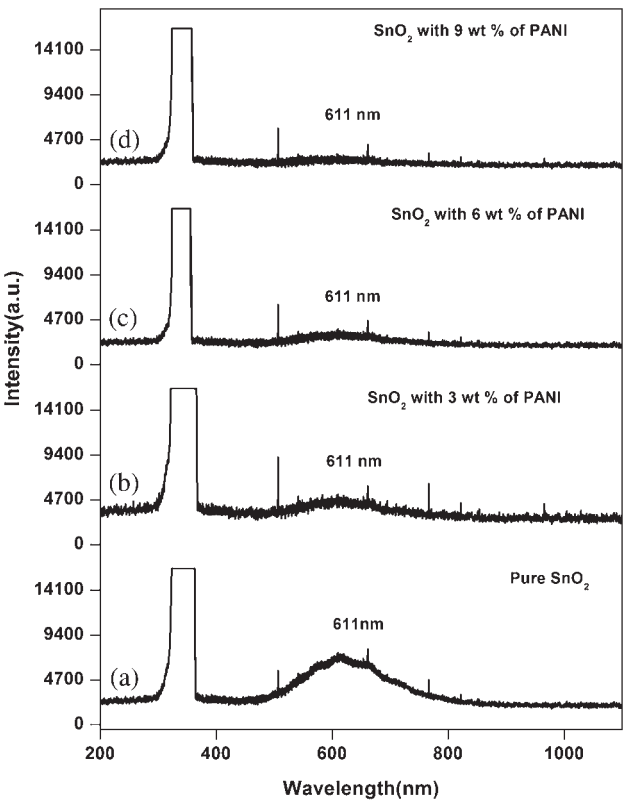

Figure 5. PL spectra of (**a**) pure SnO_2, (**b**) 3 wt%, (**c**) 6 wt% and (**d**) 9 wt% of PANI in the SnO_2/PANI nanocomposite.

broad emission peak centred at 611 nm (1.875 eV) is observed in all samples. The intensity of this broad peak has been found to decrease with increasing weight per cent of PANI in SnO_2. The gradual decrease of the intensity (flattening) of the PL signal (611 nm) may be associated with the decreased density of oxygen vacancies (V_O) on the surface of SnO_2/PANI nanocomposites. The surface of the nanocomposite pellets of SnO_2 with 9 wt% of PANI seems to be defect-free (oxygen vacancies) due to the charge transfer from PANI. These results are consistent with the fact that the variations in the luminescence of SnO_2 pellets originate from the surface electronic energy states due to the surface oxygen vacancies (V_O) created by many types of surface oxygen deficiencies located in different regions of the surface of the samples. These results, i.e. the surface free from oxygen vacancies are consistent with the sheet carrier concentration measurements on the SnO_2/PANI nanocomposite samples which are presented in table 3.

3.5 *Hall measurement analysis*

The electrical properties of pure SnO_2 and SnO_2/PANI nanocomposites with different wt% loading of PANI (3, 6, 9 wt%) and pure PANI were measured at room temperature (300 K) and are presented in table 3. The electrical conductivities of pure SnO_2, PANI and SnO_2/PANI nanocomposites were found to be 9.412×10^{-10}, 1.383×10^{-5} and $1.391 - 1.441 \times 10^{-6}\ \Omega^{-1}\ cm^{-1}$, respectively. It is evident from table 3 that after the addition of PANI in the SnO_2 nanoparticle matrix, the electrical conductivity increases by four orders of magnitude with respect to pure SnO_2. This

Table 3. Electrical properties of pure SnO_2, its nanocomposites SnO_2/PANI with different wt% loading of PANI (3, 6, 9 wt%) in pure SnO_2.

Samples	Bulk carrier concentration $(N_b)/cm^3$	Mobility (μ), $cm^2/V/s$	Resistivity (ρ), Ω cm	Hall coefficient (R_H)	Surface carrier concentration $(N_s)/cm^3$	Conductivity (σ), Ω^{-1} cm^{-1}
Pristine SnO_2	9.002×10^{12}	6.527×10^{-4}	1.062×10^{9}	-6.934×10^{5}	6.301×10^{8}	9.412×10^{-10}
$SnO_2 + 3$ wt% of PANI	4.449×10^{12}	1.952×10^{0}	6.988×10^{5}	-1.403×10^{6}	3.114×10^{8}	1.391×10^{-6}
$SnO_2 + 6$ wt% of PANI	3.506×10^{12}	2.554×10^{0}	6.971×10^{5}	-1.780×10^{6}	2.455×10^{8}	1.434×10^{-6}
$SnO_2 + 9$ wt% of PANI	1.011×10^{12}	8.895×10^{0}	6.941×10^{5}	-6.174×10^{6}	7.077×10^{7}	1.441×10^{-6}
Pure PANI	2.075×10^{11}	4.160×10^{2}	7.232×10^{4}	$+3.008 \times 10^{7}$	1.453×10^{7}	1.383×10^{-5}

change of conductivity may be associated with the four orders of magnitude increment in carrier mobility (μ) from 6.527×10^{-4} $cm^2/V/s$ of pure SnO_2 to 8.895×10^{0} $cm^2/V/s$ of SnO_2/PANI (9 wt%) nanocomposite. The most common protonated emeraldine salt has conductivity in the range of 10^{-5}–10^{-1} Ω^{-1} cm^{-1} [28] having a magnitude higher than common polymers ($<10^{-12}$ Ω^{-1} cm^{-1}) but lower than typical metals ($>10^{-1}$ Ω^{-1} cm^{-1}). Also, emeraldine base (PANI-EB) can be made conductive by adding a protonic acid dopant via a mechanism [29] in which the dissociation of bipolaron occurs to produce two polarons. By the augmentation of organic or inorganic pollutants into the primary polymers, an increase in the conductivity of the resulted composite material was observed [30]. PANI is found in three forms but its emeraldine form is a conductor due to the protonation of the H^+ ion. Upon the electrochemical oxidation of leucoemeraldine, PANI undergoes an insulator–metal transition [31].

Conductivity (σ) is the product of the number of charge carriers (n) in a material, the mobility (μ) of these charge carriers and elementary electron charge (e) as shown in eq. (2). Resistivity (ρ) is the inverse of conductivity:

$$\sigma = e \cdot n \cdot \mu = \frac{1}{\rho}. \tag{2}$$

The number of charge carriers can be increased by doping which can be achieved by substitutional doping, creation of vacancies or the implantation of interstitials. The donor (or acceptor) state changes the electronic band structure of the material. For increased donor density, the donor state merges with the conduction band at a certain critical density n_c, whose magnitude can be predicted by Mott's criterion [32,33]:

$$n_c^{1/3} \cdot a_0^* \approx 0.25. \tag{3}$$

The effective Bohr radius a_0^* is given by

$$a_0^* = \frac{h^2 \varepsilon_0 \varepsilon^m}{\pi e^2 m_c^*}. \tag{4}$$

From the above observations, it is inferred that by the addition of PANI in bulk SnO_2 (which is a good insulator), the electrical conductivity and carrier mobility can be enhanced by at least four orders of magnitude. Also, the surface carrier concentration which is much less than the bulk carrier concentration (N_b) can be decreased at least by one order of magnitude by the dispersion (addition) of PANI in the SnO_2 matrix. By decreasing the surface carrier concentration (N_s), the surface energy defects due to oxygen vacancies in SnO_2 can also be minimised.

4. Conclusions

In this study, a series of tin oxide (SnO_2)/PANI nanocomposites with loading of different wt% (3, 6, 9 wt%) of PANI were synthesised using a solution-based processing technique in an attempt to enhance the structural, electrical and optical properties of SnO_2. The effect of the addition of PANI on the gross structure, surface morphology, chemical composition, nature of chemical bonds, optical properties and electrical properties of SnO_2/PANI nanocomposites was investigated. The surface morphological study by SEM exhibits the homogeneous dispersion of PANI in the tin oxide matrix where the gross/average structure remains unchanged as revealed by PXRD. The shape and size of SnO_2 nanoparticles are spherical and are in the range of 200–500 nm, respectively. The lattice parameters of the pristine rutile crystalline structure of SnO_2 are found to be $a = b = 4.7328$ Å, $c = 3.1838$ Å and a slight change has been recorded in the lattice constants of the SnO_2/PANI nanocomposites. However, the crystallite size has been found to decrease from 60 to 40 nm with the different wt% loading of PANI. The presence of Fourier transform infrared (FT-IR) peaks corresponding to the chemical bonds such as C–H, C=C, NH_2, C–C and the EDAX spectrum confirms the formation of the SnO_2/PANI nanocomposites. The PL spectroscopic study shows a broad emission peak at

611 nm for both pure SnO_2 and SnO_2/PANI nanocomposites with a gradual decrement in intensity due to the disappearance of the surface defects associated with oxygen vacancies. The uniform dispersion of PANI at the nanoscale significantly enhanced the electrical properties by Hall measurement, e.g., at least four orders of magnitude changes in the DC electrical conductivity and carrier mobility.

Acknowledgements

The authors are thankful to Prof. Poonam Tandon, Department of Physics, University of Lucknow, Uttar Pradesh for her assistance in recording the FT-IR spectra and Dr K Ashokan and Dr M Saif, Inter-University Accelerator Centre, New Delhi for providing the facilities of the I–V curve/Hall measurement and the scanning electron microscope.

References

[1] V Natalia Blinova and J Stejskal, *Polym. Int.* **57**, 66 (2008)
[2] S Sedaghat and M S Alavijeh, *Int. Nano Lett.* **4**, 115 (2014)
[3] V H Nguyen, L Tang and J J Shim, *Colliod Polym. Sci.* **291**, 2237 (2013)
[4] B G Soares, F G Souza Jr, A Manjunath, H Somashekarappa, R Somashekar and Siddaramaiah, *Pramana – J. Phys.* **69**, 435 (2007)
[5] T Puzyn, D Leszczynska and J Leszczynski, *Adv. Chalk. Small* **5**, 2494 (2009)
[6] J Leszczynski, *Nat. Nanotechnol.* **5**, 633 (2010)
[7] S Sarmah and A Kumar, *Bull. Mater. Sci.* **36**, 31 (2013)
[8] S Vohra, M Kumar, M L Singla and S K Mittal, *J. Mater. Sci.* **24**, 1354 (2013)
[9] O Kamigaito, *J. Jpn. Soc. Powder Metal.* **38**, 315 (1991)
[10] M Fernandez Garcia, A Martínez-Arias, J C Hanson and J A Rodríguez, *Chem. Rev.* **104**, 4063 (2004)
[11] C Kilic and A Zunger, *Phys. Rev. Lett.* **88**, 095501 (2002)
[12] A Alam, A Ansari, M Rafi Shaik and M Alandis, *Arabian J. Chem.* **6**, 341 (2013)
[13] S C Raghvendra, S Khasim, M Revanasiddappa, M V N A Prasad and A B Kulkarni, *Bull. Mater. Sci.* **26**, 733 (2003)
[14] L N Korosi, S Pupp, V Meynen, P Cool, E F Vansont and I Dekany, *Colloids Surf. B* **268**, 147 (2005)
[15] H Zhang, N Du Chen, T Cui and D Yang, *Mater. Res. Bull.* **43**, 3164 (2008)
[16] C J Brabee, N S Sariciftei and J C Hummelen, *Adv. Funct. Mater.* **11**, 15 (2001)
[17] H Bai and G Shi, *Sensors* **7**, 267 (2007)
[18] S Virji, J Huang, R B Kanver and B H Weiller, *Nano Lett.* **4**, 491 (2004)
[19] G Yu, J Gao, J G Hummelen, F Wudl and A J Heeger, *Science* **270**, 1789 (1995)
[20] N G Desphande, Y G Gudege, R Sharma, J C Vyas, J B Kim and Y P Lee, *Sens. Actuators B* **138**, 76 (2009)
[21] B K Sharma, A K Gupta, N Khare, S K Dhawan and H C Gupta, *Synth. Metal* **159**, 391 (2009)
[22] K Dutta and S K De, *Mater. Lett.* **61**, 4967 (2007)
[23] M A Khan, M K Uddin, R Bushra, A Ahmad and S A Nabi, *React. Kinet. Mech. Cat.* **113**, 499 (2014)
[24] C Mayyoso, S K Manohar, A C Macdiarmid and A J Epstein, *J. Polym. Sci.* **33(A)**, 1227 (1995)
[25] R Murugesan and E Subramanian, *Bull. Mater. Sci.* **25**, 613 (2002)
[26] V G Bairi, B A Warford, S E Bourdo, A S Biris and T J Viswanathan, *J. Appl. Polym. Sci.* **124**, 3320 (2012)
[27] N V Hieu, N Q Dung, P D Tam, T Trung and N D Chien, *Sens. Actuators B-Chem.* **140**, 500 (2009)
[28] M Trchova, J Zemek and J Stejskal, *Macromolecules* **31**, 2218 (1998)
[29] J Stejskal and R G Gilbert, *Pure Appl. Chem.* **74**, 857 (2002)
[30] S K Patel, R B Patel, A Awadhia, N Chand and S L Agrawal, *Pramana – J. Phys.* **69**, 467 (2007)
[31] H L Wu and Philip Phillips, *Phys. Rev. Lett.* **66**, 1366 (1991)
[32] N F Mott, *Can. J. Phys.* **34**, 1356 (1956)
[33] N F Mott, *Philos. Mag.* **6**, 1013 (1961)